Available online at www.sciencedirect.com
SCIENCE DIRECT®
Nuclear Physics B (Proc. Suppl.) 134 (2004) 39–46
NUCLEAR PHYSICS B PROCEEDINGS SUPPLEMENTS
www.elsevierphysics.com

The Space Experiment PAMELA

M. Boezio[a] *, V. Bonvicini[a], E. Mocchiutti[a], P. Schiavon[a], A. Vacchi[a], G. Zampa[a], N. Zampa[a], A. Bakaldin[b], A.M. Galper[b], S.V. Koldashov[b], M.G. Korotkov[b], V.V. Mikhailov[b], S.A. Voronov[b], Y. Yurkin[b], A. Basili[c], R. Bencardino[c], L. Bongiorno[c], M. Casolino[c], M.P. De Pascale[c], G. Furano[c], A. Menicucci[c], M. Minori[c], A. Morselli[c], P. Picozza[c], R. Sparvoli[c], R. Wischnewski[c], O. Adriani[d], L. Bonechi[d], M. Bongi[d], F. Giambi[d], P. Papini[d], S.B. Ricciarini[d], P. Spillantini[d], S. Straulino[d], F. Taccetti[d], E. Vannuccini[d], G. Castellini[e], P. Carlson[f], J. Lund[f], J. Lundquist[f†], S. Orsi[f], M. Pearce[f], G.C. Barbarino[g], D. Campana[g], G. Osteria[g], G. Rossi[g], S. Russo[g], M. Boscherini[h], W. Menn[h], M. Simon[h], M. Ricci[i], M. Ambriola[j], R. Bellotti[j], F. Cafagna[j], M. Circella[j], C. De Marzo[j], N. Giglietto[j], N. Mirizzi[j], M. Romita[j], P. Spinelli[j], E. Bogomolov[k], S. Krutkov[k], G. Vasiljev[k], G. Bazilevskaja[l], A. Grigorjeva[l], R. Mukhametshin[l], Y. Stozhkov[l], J.W. Mitchell[m], R.E. Streitmatter[m], S.J. Stochaj[n]

[a]INFN, Structure of Trieste and Physics Department of University of Trieste, Trieste, Italy

[b]Moscow Engineering and Physics Institute, Moscow, Russia

[c]INFN, Structure of Rome II and Physics Department of University of Rome "Tor Vergata", Rome, Italy

[d]INFN, Structure of Florence and Physics Department of University of Florence, Florence, Italy

[e]Istituto di Fisica Applicata "Nello Carrara", Italy

[f]Royal Institute of Technology (KTH), Stockholm, Sweden

[g]INFN, Structure of Naples and Physics Department of University of Naples "Federico II", Naples, Italy

[h]Universität Siegen, Siegen, Germany

[i]INFN, Laboratori Nazionali di Frascati, Frascati, Italy

[j]INFN, Structure of Bari and Physics Department of University of Bari, Bari, Italy

[k]Ioffe Physical Technical Institute, Russia

[l]Lebedev Physical Institute, Russia

[m]NASA/Goddard Space Flight Center, Greenbelt, (USA)

[n]New Mexico State University, Las Cruces, (USA)

We present in this paper a status report of the space experiment PAMELA. PAMELA is a satellite-borne experiment which primarily aims to measure the antiproton and positron spectra in the cosmic radiation over a large energy range (from 80 MeV up to 190 GeV for antiprotons and from 50 MeV up to 270 GeV for positrons) and to search for antinuclei with a sensitivity of the order of 10^{-8} in the antihelium/helium ratio. In addition, it will measure the light nuclear component of cosmic rays and investigate phenomena connected with Solar and Earth physics. The apparatus will be installed onboard the polar orbiting Resurs DK1 satellite, which will be launched into space by a Soyuz TM2 rocket in 2004 from Baikonur cosmodrome in Kazakhstan, for a 3 year long mission. PAMELA consists of: a time of flight system, a transition radiation detector, a magnetic spectrometer, an anticoincidence detector, an electromagnetic imaging calorimeter, a shower tail catcher scintillator and a neutron detector.

0920-5632/$ – see front matter
doi:10.1016/j.nuclphysbps.2004.08.006

1. Introduction

The PAMELA experiment (a Payload for Antimatter Matter Exploration and Light-nuclei Astrophysics) is the main part of a scientific program of the WiZard collaboration, which aims to measure the cosmic radiation and its composition. Several missions have already been carried out both with balloon-borne [1] and satellite-borne [2] experiments.

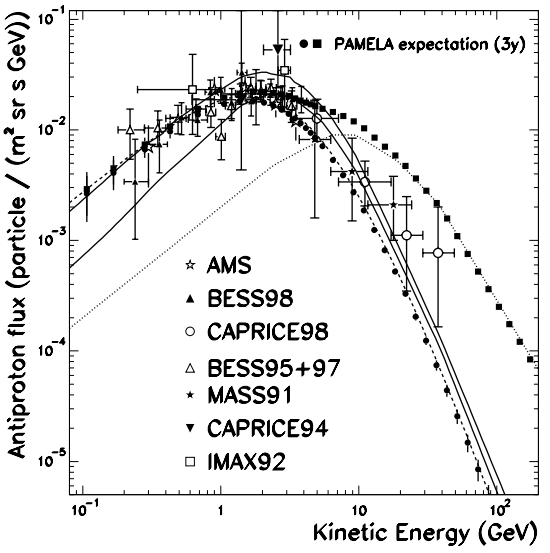

Figure 1. Several recent experimental $\overline{p}$ spectra (AMS[11], BESS98[12], CAPRICE98[1], BESS95+97[13], MASS91[14], CAPRICE94[15], IMAX92[16]) along with theoretical calculations for a pure $\overline{p}$ secondary production (solid lines: [5], dashed line: [6]) and for a pure $\overline{p}$ primary production (dotted line: [9]). The expected PAMELA performances, in case of a pure secondary component (filled circles) and of a primary component (filled boxes), are indicated. Only statistical errors are included in the expected PAMELA data.

PAMELA is a satellite-borne experiment designed to study charged particles in the cosmic radiation. It will be mounted in a pressurized vessel attached to a Russian Earth-observation satellite, the Resurs DK1, that will be launched into space by a Soyuz TM2 rocket in 2004 from Baikonur cosmodrome, in Kazakhstan. The orbit will be elliptical and semi-polar, with an inclination of 70.4° and an altitude varying between 350 km and 600 km.

During its at least three-year long mission, PAMELA will measure with high precision the energy spectrum and the composition of the cosmic radiation, in particular looking for its antimatter component.

2. Scientific objectives

The main objectives of the experiment are the precise measurement of the positron flux from 50 MeV to 270 GeV and the antiproton flux from 80 MeV to 190 GeV. These measurements are very interesting because at low energies (below a few GeV) solar modulation effects and the existence of primary components such as evaporation of primordial black holes (e.g. see [3]) and at high energies (above 10 GeV) acceleration and propagation mechanisms in the Galaxy plus possible primary components due to annihilation of supersymmetric particles (e.g. see [4]) or extragalactic components can be probed. Figures 1 and 2 show the current status of the cosmic-ray antiproton and positron measurements, respectively, along with some theoretical calculations for a pure secondary antiproton and positron production ([5–8]) and for a pure primary antiproton and positron production due to annihilation of supersymmetic particles ([9,10]). Almost all data available so far have been obtained by balloon-borne experiments. The short data-taking time (approximately 24 hours) and the presence of a residual overburden of atmosphere above the detecting apparatus at the altitudes that a balloon can reach (around 40 km, $\sim$5 g/cm^2 of residual atmosphere) are the main limits of such kind of measurements. PAMELA

*corresponding author, e-mail:mirko.boezio@ts.infn.it
†now at INFN, Structure of Trieste, Trieste, Italy

will be able to perform very precise measurements with high statistics ($\sim 10^4$ $\overline{\mathrm{p}}$ and $\sim 10^5$ e^+ per year) and over a wider range of energy than ever reached before. The filled circles indicates the expected PAMELA performance in case of a pure secondary antiproton component (Figure 1) and the full boxes the expected performance in case of a primary component (Figures 1 and 2).

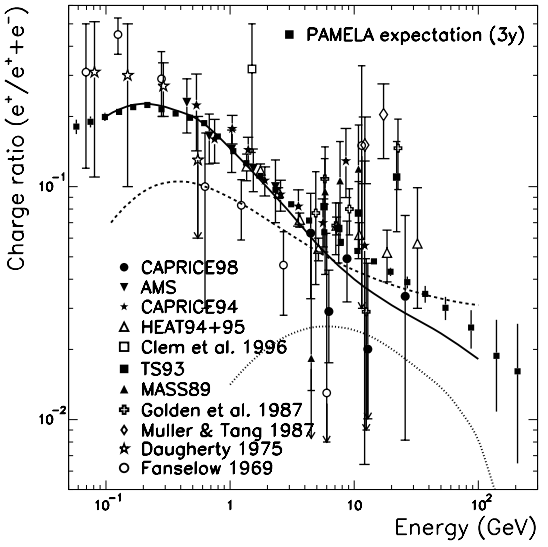

Figure 2. The positron fraction as a function of energy measured by several experiments ([17–21] and MASS89[22], TS93[23], HEAT[24], CAPRICE94[25], AMS[26], CAPRICE98[27]). The dashed [7] and the solid [8] lines are calculation of the secondary positron fraction. The dotted line is a possible contribution from annihilation of neutralinos of mass 336 GeV [10]. The expected PAMELA performance, in case of a primary component, is indicated (filled boxes). Only statistical errors are included in the expected PAMELA data.

PAMELA will also search for light antinuclei in cosmic rays, measuring the $\overline{\mathrm{He}}$/He ratio with a sensitivity $\sim 10^{-8}$, and it will measure the spectra of various components of the cosmic radiation such as protons, electron and light nuclei up to Z=6.

The nearly polar orbit and low momentum threshold of PAMELA will permit to study solar modulation effects and to measure the electron, positron and proton high energy component of solar flares. Furthermore, it will be possible to study the effect of the Earth magnetic field on the cosmic radiation.

3. The PAMELA apparatus

The apparatus is composed of the following subdetectors, arranged as in Figure 3, from top to bottom:

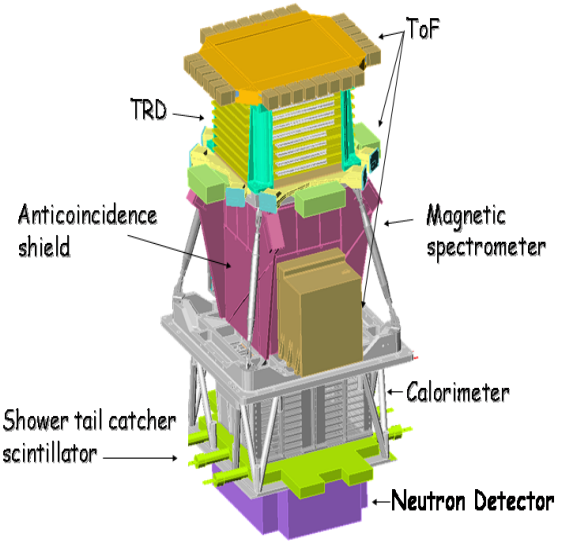

Figure 3. The PAMELA telescope.

- a time of flight system (ToF);

- a transition radiation detector (TRD);
- a magnetic spectrometer;
- an anticoincidence system;
- an electromagnetic imaging calorimeter;
- a shower tail catcher scintillator;
- a neutron detector.

The detector is approximately 130 cm high, has a mass of about 470 kg and the power consumption is 360 W.

3.1. The time of flight system

The Time-of-Flight system [28] is composed of 6 layers of segmented plastic scintillators arranged in three planes, located as indicated in Figure 3, and read out by photomultiplier tubes.

The ToF provides a fast signal for triggering the data acquisition in the other subdetectors, determines the absolute value of the charge Z of incident particles through multiple measurements of the energy loss in the planes and measures the flight time of particles crossing its planes.

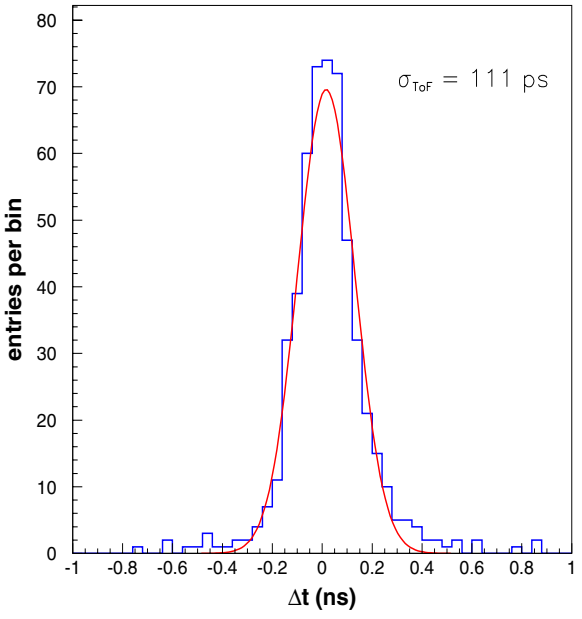

Figure 4. Timing resolution for a time–of–flight paddle, after correcting for time–walk.

Figure 4 shows the distribution of the differences (converted to a time) between the impact points of cosmic-ray particles at ground on a ToF paddle reconstructed by the ToF and the ones obtained using an external drift chamber. Time walk corrections were applied to the data. The resulting timing resolution allows for a separation between antiprotons (protons) and electrons (positrons) up to about 1.5 GeV.

3.2. Transition Radiation Detector

The TRD [29] is a detector made up of 10 carbon-fiber radiator layers interleaved with 9 planes of Xe-CO_2 straw tubes working in a proportional regime at a voltage of 1400 V, arranged in a truncated pyramid shape. A single straw tube is 28 cm in length and 4 mm in diameter. It is made of a copper kapton foil, 25 μm thick, with a tungsten anode wire inside, 25 μm in diameter, stretched up to a 60 g stress.

Relativistic particles crossing boundaries of materials with different dielectric constant (the radiator layers interfaces) will emit transition radiation in the X-ray range, which is then revealed by the gas detectors. By measuring this radiation it is possible to separate electrons and positrons from heavier particles. Using data collected during test beams at CERN it was found [29] that the PAMELA TRD can separate electrons from protons with an efficiency of 90% and a contamination of about 5% in the energy range of interest for PAMELA.

3.3. Magnetic Spectrometer

The central part of PAMELA apparatus is a magnetic spectrometer [30] consisting of a permanent magnet and a silicon tracker.

The magnet is composed by 5 modules of a sintered Nd–Fe–B alloy with a residual magnetic induction of about 1.3 T. The tracking cavity is 445 mm tall and has a cross–section of 132 mm $\times$ 162 mm, which results in a geometrical factor for the experiment of 20.5 cm^2sr. The particular magnetic configuration results in a nearly

uniform magnetic field inside the spectrometer cavity of about 0.4 T.

The tracking system is composed of 6 detecting planes interleaved with the magnetic modules. Each plane is made up of 6 double–sided microstrip silicon detectors, 300 μm thick. The strip pitch is 25 μm for the junction side (which is used to measure the coordinate in the bending plane, X view, of the particles inside the magnetic cavity) and one strip out of two is connected to the read–out electronics. On the Ohmic side the pitch is 67 μm, strips are orthogonally implanted with respect to the previous ones. This configuration gives a total of 6144 read–out channels for each of the 6 planes. In order to reduce the amount of data to be transmitted from the satellite a compression algorithm has been developed. The compression factor that has been obtained is about 95%, with no degradation of the detector response.

Figures 5 and 6 show a 100 GeV/c e^- and p event, respectively, from test beam data as detected by the tracking system and the calorimeter. The clear track signatures in the spectrometer can be seen.

Figure 7 shows the momentum resolution as a function of momentum obtained using electrons from test beam data. The resolution is due to a combination of two effects: multiple scattering and finite measurement resolution, which can be parameterized as:

$$\sqrt{a^2 + b^2 \times p^2}$$

with $a = (3.22 \pm 0.44) \times 10^{-2}$ representing the component due to the multiple scattering and $b = (0.845 \pm 0.038) \times 10^{-3}$ $(\mathrm{GeV}/c)^{-1}$ the component due to the finite measurement resolution. From this the Maximum Detectable Rigidity, i.e. the rigidity for which the error is 100%, results: (1183 ± 54) GV/c.

3.4. Anticounter System

The anticounter system [31] consists of four lateral detectors covering the sides of the tracker and one top detector above the tracker. Each detector is made from a sheet of plastic scintillator read out by multiple compact photomultiplier tubes, equipped with a LED based system for in–flight checks.

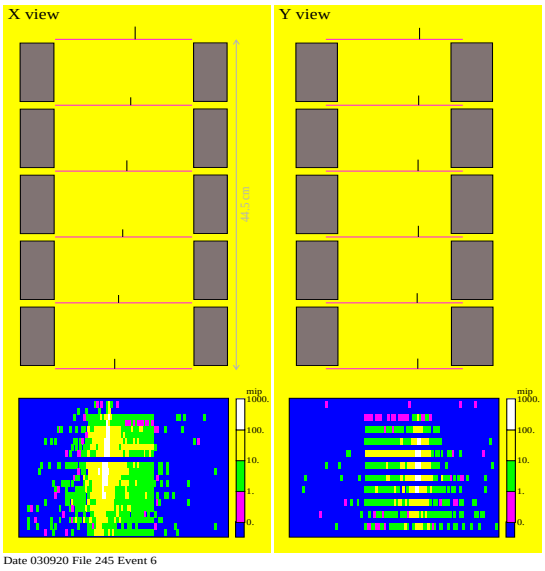

Figure 5. The event display of a 100 GeV/c e^- from test beam data in the PAMELA tracking system and calorimeter. The signals from the odd planes of the Y view of the calorimeter (right side) were not read-out at this test beam.

The anticounter system is used both to identify and to reject multiparticle events offline and in an on-board second level trigger [32] to reject events not fully contained in the PAMELA acceptance.

The efficiency for detecting minimum ionizing particles has been measured using cosmic ray muons and it has been found to exceed 99.9% per detector.

3.5. Electromagnetic Imaging Calorimeter

The sampling calorimeter is made of silicon sensor planes interleaved with plates of tungsten absorber [33]. Each tungsten layer has a thickness of 0.26 cm, which corresponds to 0.74 X_0 (radiation lengths). Since there are 22 tungsten layers, the total depth is 16.3 X_0 (about 0.6 interaction lengths).

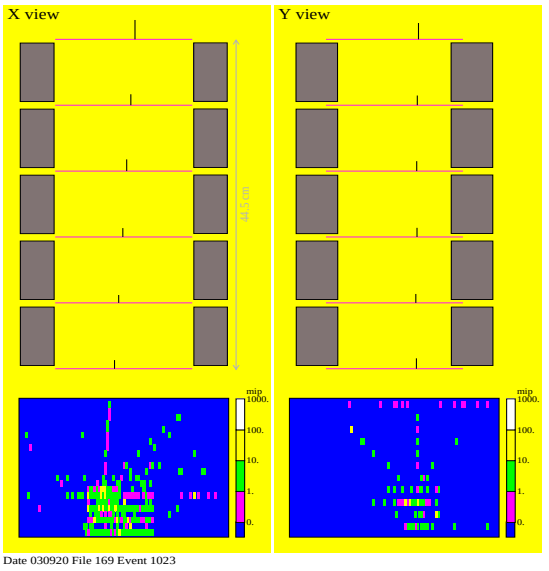

Figure 6. The event display of a 100 GeV/c p from test beam data in the PAMELA tracking system and calorimeter. The signals from the odd planes of the Y view of the calorimeter (right side) were not read-out at this test beam.

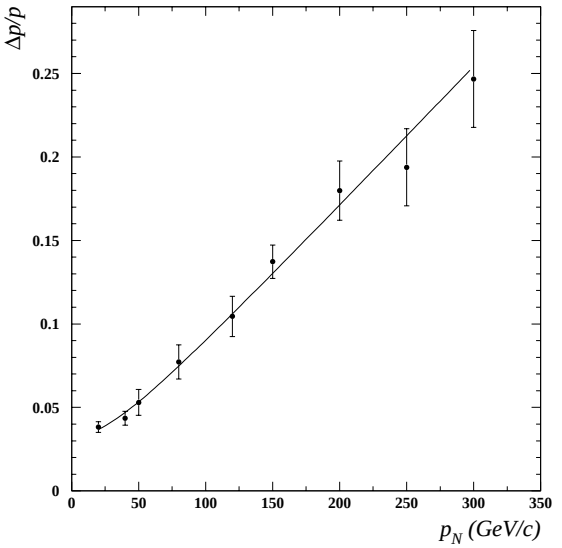

Figure 7. The spectrometer momentum resolution as a function of momentum using test beam electron data.

Each tungsten plate is sandwiched between two printed circuit boards (called "front-end boards"), which house the silicon detectors and the front-end and ADC electronics. The silicon detectors developed for the calorimeter are large area devices (8x8 cm^2) and each of them is segmented into 32 large strips with a pitch of 2.4 mm and has a thickness of 380 μm. In each front-end board the detectors are arranged in a square matrix of 3×3 devices and each of the 32 strips of a detector is wire-bonded to the corresponding one of the other two detectors in the same row (or column), thus forming 24 cm-long strips. The orientation of the strips of two consecutive layers is rotated by 90° to provide 2-dimensional spatial informations.

As can been noticed from the e$^-$ and p events displayed in Figures 5 and 6 the simultaneous measurement of energy and topology of the crossing particles allows an high identification power for electromagnetic showers. Figure 8 shows the number of strips hit in the calorimeter as a function of total detected energy for 200 GeV/c test beam electrons and protons. A clear separation between the two type of particles can be seen. Furthermore, other topological information, such as, for example, the fraction of energy lost in a cylinder of radius 1.5 strip around the track of the primary particle, can be used for the identification. This variable is depicted in Figure 9 for 200 GeV/c e$^-$ (solid histograms) and for p (dashed histograms) before (a) and after (b) a selection based on the total energy (from Figure 8).

Combining all topological and energetic information available from the calorimeter a rejection factor better than 10^4 for protons and electrons at 95% selection efficiency in positron and antipro-

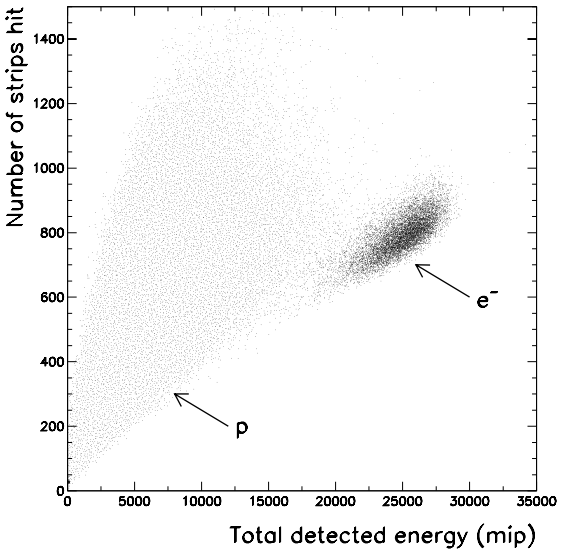

Figure 8. The total number of strips hit versus the total detected energy in the calorimeter for 200 GeV/c e^- and p data taken at the SPS test beam.

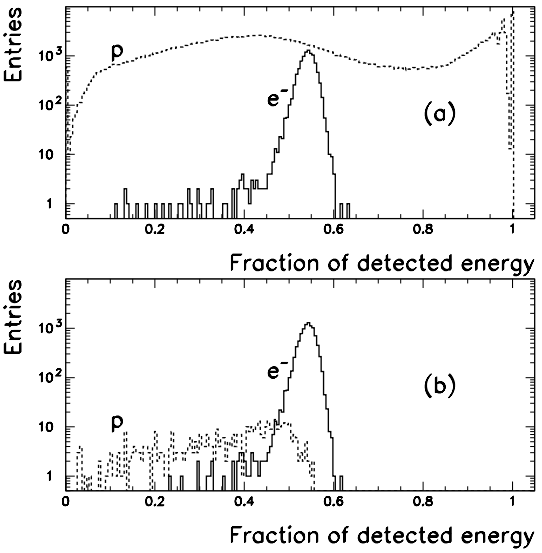

Figure 9. Fraction of energy lost in a cylinder of radius 1.5 strip around the track of the primary particle for test beam data (200 GeV/c e^- and p). (a) The complete set of data; (b) the events surviving a selection based on the total detected energy.

ton measurements can be obtained in the energy range of interest for PAMELA.

The calorimeter can also be operated in self–trigger mode [33]: this hardware feature allows the stand–alone detection of $e^{\pm}$ with an increased acceptance of 470 cm^2sr up to an energy ~ 2 TeV and an energy resolution $\simeq 12\%$.

3.6. Shower tail catcher scintillator

The detector is made of a single square scintillator paddle 482×482 mm^2 wide and 10 mm thick readout by six photomultipliers. These are placed three by three on two opposite sides of the scintillator, have an overall efficiency of about 99.97 ± 0.02 and a dynamic range of $1\div1000$ mip.

The scintillator is located below the calorimeter to detect particles escaping from it and to provide an additional trigger for high energy (> 100 GeV) electrons.

3.7. Neutron detector

The purpose of this detector is to complement the electron-proton discrimination capabilities of the PAMELA TRD and calorimeter detecting the much larger neutron production due to hadronic showers than to electromagnetic ones in the calorimeter. Furthermore, the joint analysis of the calorimeter and neutron detector information will allow to identify primary electrons at energies up to 10 TeV.

The detector is made of proportional counters, filled with ^{3}He, surrounded by a polyethylene moderator enveloped in a thin cadmium layer. The 36 counters are stacked in two planes of 18 counters each, oriented along the Y-axis of the instrument. The size of the neutron detector is $600 \times 550 \times 150$ mm^3.

4. Conclusions

PAMELA is a powerful instrument that will give results of great scientific relevance in several fields of cosmic ray research. Extensive space qualification tests of PAMELA detectors, electronics and mechanical structures have been developed and are still in progress. Final qualification tests on the mass and thermal model of the PAMELA apparatus has just been completed at the TsSKB–Progress factory in Samara, Russia. The engineering model of PAMELA has been completed and shown to be fully compliant with the requirements of the Resurs DK1 spacecraft environment.

The detectors have been extensively tested both at PS and SPS beams at CERN and shown to comply with their design performance.

The integration of the flight model of PAMELA is underway in Rome. Its delivery to TsSKB–Progress for integration with the Resurs DK1 satellite is foreseen for early spring 2004 and the launch is scheduled for the second half of 2004.

REFERENCES

1. M. Boezio et al., Astrophys. J. 561 (2001) 787
2. V. Bidoli et al., Astrophys. J. Suppl. 132 (2001) 365.
3. K. Maki, T. Mitsui, T., and S. Orito, Phys. Rev. Lett. 76 (1996) 3474.
4. L. Bergström, J. Edsjö and P. Ullio, Phys. Rev. D 59 (1999) 43506.
5. M. Simon, A. Molnar and S. Roesler, Astrophys. J. 499 (1998) 250.
6. L. Bergström and P. Ullio, private communication (1999).
7. R. J. Protheroe, Astrophys. J. 254 (1982) 391.
8. I. V. Moskalenko and A. W. Strong, Astrophys. J. 493 (1998) 694.
9. P. Ullio, astro-ph/9904086 (1999).
10. E. A. Baltz and J. Edsjö, Phys. Rev. D 59 (1999) 023511.
11. M. Aguilar et al., Phys. Rept. 366 (2002) 331.
12. T. Maeno et al., Astropart. Phys. 16 (2001) 121
13. S. Orito et al., Phys. Rev. Lett. 84 (2000) 1078.
14. G. Basini et al., Proc. 26th International Cosmic Ray Conference (Salt Lake City, 1999) 4, 77; see also M. Hof et al., Astrophys. J. 467 (1996) L33.
15. M. Boezio et al., Astrophys. J. 487 (1997) 415.
16. J. Mitchell et al., Phys. Rev. Lett. 76 (1996) 3057.
17. J. L. Fanselow, R. C. Hartman, R. H. Hildebrand and P. Meyer, Astrophys. Jour. 158 (1969) 771.
18. J.K. Daugherty, R.C. Hartman and P.J. Schmidt, Astrophys. Jour. 198 (1975) 493.
19. R. L. Golden et al., Astrophys. J. 287 (1984) 622.
20. D. Müller and K. K. Tang, Astrophys. J. 312 (1987) 183.
21. J. M. Clem et al., Astrophys. J. 464 (1996) 507.
22. R. L. Golden et al., Astrophys. J. 436 (1994) 769.
23. R. L. Golden et al., Astrophys. J. 457 (1994) L103.
24. S. W. Barwick et al., Astrophys. J. 498 (1998) 779.
25. M. Boezio et al., Astrophys. J. 532 (2000) 653; see also G. Barbiellini et al., Astron. Astrophys. 309 (1996) L15.
26. J. Alcaraz et al., Phys. Lett. B 484 (2000) 10.
27. M. Boezio et al., Advances in Space Research 27 (2001) 669.
28. D. Campana et al., Proc. 28th International Cosmic Ray Conference, (Tsukuba, Japan, 2003) 2141.
29. F. Cafagna et al., Proc. 28th International Cosmic Ray Conference (Tsukuba, Japan, 2003) 2121.
30. O. Adriani et al., Nucl. Instr. and Meth. A 511 (2003), 72
31. M. Pearce et al., Proc. 28th International Cosmic Ray Conference (Tsukuba, Japan, 2003) 2125.
32. J. Lundquist et al., Proc. 28th International Cosmic Ray Conference (Tsukuba, Japan, 2003) 2133.
33. M. Boezio et al., Nucl. Instr. and Meth. A 487 (2002) 407.